

SMV-EAR: Bring Spatiotemporal Multi-View Representation Learning into Efficient Event-Based Action Recognition

Rui Fan Weidong Hao

Abstract

Event cameras action recognition (EAR) offers compelling privacy-protecting and efficiency advantages, where temporal motion dynamics is of great importance. Existing spatiotemporal multi-view representation learning (SMVRL) methods for event-based object recognition (EOR) offer promising solutions by projecting H - W - T events along spatial axis H and W , yet are limited by its translation-variant spatial binning representation and naive early concatenation fusion architecture. This paper reexamines the key SMVRL design stages for EAR and propose: (i) a principled spatiotemporal multi-view representation through translation-invariant dense conversion of sparse events, (ii) a dual-branch, dynamic fusion architecture that models sample-wise complementarity between motion features from different views, and (iii) a bio-inspired temporal warping augmentation that mimics speed variability of real-world human actions. On three challenging EAR datasets of HARDVS, DailyDVS-200 and THU-EACT-50-CHL, we show +7.0%, +10.7%, and +10.2% Top-1 accuracy gains over existing SMVRL EOR method with surprising 30.1% reduced parameters and 35.7% lower computations, establishing our framework as a novel and powerful EAR paradigm.

1. Introduction

Event cameras perceive luminance changes asynchronously with high temporal resolution ($\sim 1\mu\text{s}$), appearance-free streaming and low power consumption (Gallego et al., 2020; Chakravarthi et al., 2024; Miao et al., 2019; Steffen et al., 2024; Deng et al., 2021; Wang et al., 2024a). Existing state-of-the-art (SOTA) event-based action recognition (EAR) methods convert H - W - T ¹ sparse events into frame-like rep-

¹In this paper, we use H, W, T to denote the spatiotemporal resolution and H, W, T to denote the spatiotemporal dimensions (or axes).

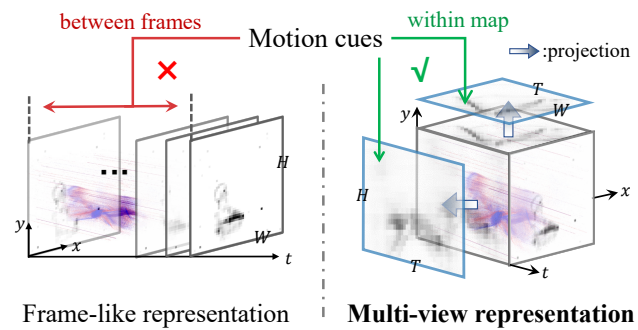


Figure 1. Comparison of frame-like representation in prior SOTA EAR method (left) and our adopted multi-view representation (right). Our SMV-EAR embeds motion cues within T - H and T - W maps rather than between H - W frames.

resentations through temporal binning² (Fig. 1 left) then adapt well-trained 2D models (Wang et al., 2024a;b; Xie et al., 2024). Although familiar to human vision, however, this practice embeds the fundamental temporal motion cues between the evolving frames over T axis with limited frame count, which may fall short in fully capturing and modeling physically continuous human actions (Li et al., 2019; Wang et al., 2024b).

To tackle this, we propose a **Spatiotemporal Multi-View**³ representation learning (SMVRL) framework for **EAR** task (**SMV-EAR**). As shown in Fig. 1 right, instead of aggregating events into H - W (Height-Width) frames along T axis, it projects events along H and W axes, which embeds temporal motion cues within the projected T - W (Time-Width) or T - H (Time-Height) maps rather than between the H - W frames. While unfamiliar to human beings, these 2D maps record fine-grained and discriminative complementary motion cues (Fig. 2), thereby exhibiting significant potential for achieving more accurate and efficient EAR.

However, directly applying frame-like representations for T - W and T - W views will inevitably degrade the EAR per-

²Discretize the time axis (T) into consecutive bins (Deng et al., 2021).

³'Spatiotemporal multi-view' refers to multiple viewpoints of spatiotemporal data with H - W - T dimensions, e.g. video and events (Li et al., 2019; Berahmand et al., 2025).

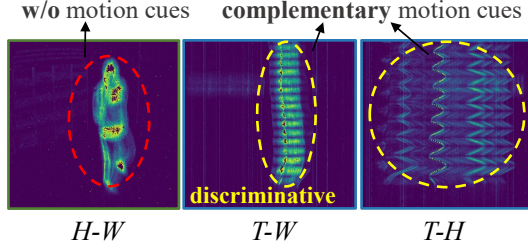


Figure 2. Projections of an action sample on different views.

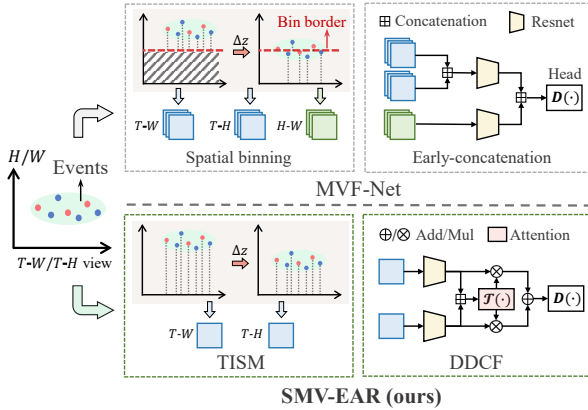


Figure 3. Comparisons of representation and architecture between baseline SMVRL method (Deng et al., 2021) (top) and our SMV-EAR (bottom). SMV-EAR ensures translation-invariant and reasonable SMVRL.

formance. This stems from two key problems: (i) An action type is expected to be independent from “where it happens” (spatial location). However, naively adapting T -axis binning for the spatial projection H/W axes (**spatial binning**) may fragment coherent action events (Fig. 3 left top), which will lead to unwanted translation-variant representations thereby resulting in poor feature discriminability (Fig. 6). (ii) Naive **early concatenation** of $T-H$ and $T-W$ maps (Deng et al., 2021) may overlook their inherent dimension misalignment (H vs. W) and semantic discrepancy (horizontal vs. vertical motion, Fig. 2), thereby failing in fully exploiting cross-view complementarity (Fig. 3 right top).

In this paper, we address these challenges by examining critical design stages of SMV-EAR: (i) By examining a plenty of basic conversion windows, measurements and aggregations (Zubić et al., 2023), we propose a **Translation-Invariant Spatiotemporal Multi-view (TISM)** representation that embeds temporal motion cues with global event count and polarity information for principled translation-invariance guarantee and compactness (Fig. 3 left bottom); (ii) By examining diverse extraction and fusion architectures, we propose a **Dual-branch Dynamic Cross-view Fusion (DDCF)** architecture that extracts view-specific action logits independently and dynamically re-weights them with cross-

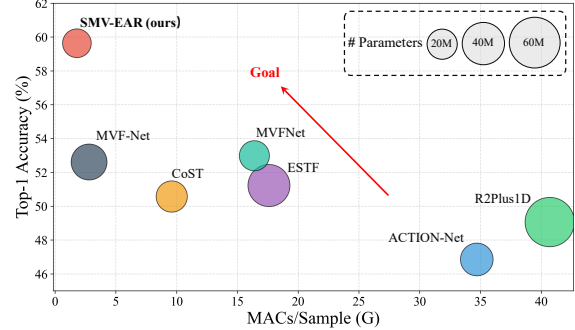


Figure 4. Results on HARDVS dataset. Our SMV-EAR surpasses all methods and sets a new performance frontier for EAR task.

view attention derived from sample-wise semantics (Fig. 3 right bottom); (iii) Consider the diverse speed variance of real-world human actions (Feichtenhofer et al., 2019), we additionally establish **Diverse Temporal Warping (DTW)** as a critical EAR augmentation that generates continuous, view-consistent action variations to further improve performance (Fig. 8).

We show on three existing most challenged EAR benchmarks, including HARDVS (Wang et al., 2024b), DailyDVS-200 (Wang et al., 2024a) and THU-EACT-50-CHL (Gao et al., 2023), that our SMV-EAR achieves +7.0%, +10.7%, and +10.2% Top-1 accuracy gains respectively, while dramatically cutting parameters by 30.1% and computations by 35.7% compared to the base line SMVRL method, MVF-Net (Deng et al., 2021) (Fig. 4). This establishes our SMV-EAR as a novel and powerful SMVRL EAR paradigm. Our main contributions can be organized as:

- While frame-like representation on $H-W$ frame is friendly for human perception, we argue that projection on $T-W, H$ views can better capture temporal motion for EAR task. We also identify two key bottlenecks, spatial binning and early concatenation for this presentation.
- We propose a SMVRL framework for EAR task, which at first uses a TISM representation to encode fine-grained temporal motion cues within maps while enabling translation-invariance. Then, a DDCF architecture is designed to exploit sample-wise complementarity between heterogeneous temporal views. Finally, we introduce the DTW, a simple but fundamental augmentation to mimic speed variability of real-world human actions.
- On challenging EAR benchmarks, our method consistently achieves significant accuracy gains over the prior SOTA methods with roughly 70% computations.

2. Related Work

2.1. Event-Based Action Recognition

Existing SOTA EAR methods convert sparse events into frame-like representations (Rebecq et al., 2017; Zhu et al., 2019; Gehrig et al., 2019) to process them with well-trained CNNs (He et al., 2016) or Video Transformers (Neimark et al., 2021; Liu et al., 2022). Despite superior in accuracy, aggregating events over discrete, limited time bins inevitably loses fine-grained temporal dynamics (Schaefer et al., 2022). Alternative point-based methods treat events as spikes (Lin et al., 2024; Ren et al., 2023; Chen et al., 2024), point clouds (Sun et al., 2025), or graphs (Xie et al., 2022; Sun et al., 2023; Deng et al., 2024) to employ architectures like SNNs (Wu et al., 2018; Tavanaei et al., 2019), point networks (Qi et al., 2017a;b), or GCNs (Fey et al., 2018; Wang et al., 2019). While efficient, these works fall short in accuracy and general hardware support (Ren et al., 2023; Fan et al., 2025). There are also works aiming to address EAR challenges under unique scenarios, such as language-guided (Zhou et al., 2024), multi-(camera)view (Gao et al., 2024), wildlife (Hamann et al., 2025), multi-modal (Steffen et al., 2024; Wang et al., 2025) and few-shot (Ruan et al., 2025) settings, yet our focus is on general human action recognition (HAR). Although beyond the scope, our SMV-EAR is orthogonal to these works thus can be integrated into them for improved performance.

2.2. SMVRL

As discussed, SMVRL offers a promising paradigm for EAR by modeling temporal dynamics from $T\text{-}H$ and $T\text{-}W$ views. However, naively adapting SMVRL methods from video analysis (Li et al., 2019; Wu et al., 2021; 2025) or EOR task (Deng et al., 2021) proves suboptimal. This is attributed to: (i) The spatial binning requirement of these methods causes an unwanted dependence between spatial location (on projection axis) of action events and the projected view maps; (ii) Their early concatenation (Deng et al., 2021) or mid-level fusion (Li et al., 2019; Wu et al., 2021) prematurely mixes features from different views characterized by distinct action semantics. Our SMV-EAR features translation-invariant representation and dynamic late-fusion architecture, which respects the semantic discrepancy of different views while exploiting their complementarity effectively.

2.3. Data Augmentation for Event Data

Existing event-based augmentations include random drops (Gu et al., 2021), spatial transformations (Li et al., 2022), occlusions (Bendig et al., 2024), meta learning (Gu et al., 2024), and mixing strategies (Shen et al., 2023; Dong et al., 2025). However, they often fail to generate complex,

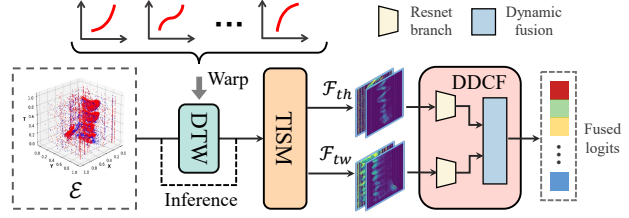


Figure 5. Overview of main contributions in SMV-EAR’s pipeline.

non-uniform temporal dynamics characterizing real-world human actions (Feichtenhofer et al., 2019). Our DTW distinguishes itself by comprehensive temporal warping functions. Moreover, video-based temporal augmentations (e.g., temporal sampling (Ramesh et al., 2023), temporal jittering (Chen et al., 2025)) operate on dense frame intervals, while our DTW directly manipulates sparse event timestamps rather than frame indices to apply non-uniform warping and ensure consistent warping across different views. This is a geometric constraint unattainable in frame-based methods.

3. Methodology

3.1. Overall Framework

Our work is built upon the principle that effective SMVRL EAR framework requires: (i) translation-invariant multi-view representation (by TISM), (ii) view-specific motion extraction and dynamic cross-view fusion (by DDCF), and (iii) diverse action variant generation (by DTW). As shown in Fig. 5, input events \mathcal{E} are converted by TISM into 2D feature maps $\{F_{th}, F_{tw}\}$ from $T\text{-}H$ and $T\text{-}W$ views. DDCF processes these maps with independent neural branches and cross-view dynamic attention fusion to predict action types. Finally, DTW augmentation further enhances test accuracy.

3.2. Translation-invariance of TISM

Formulation. Let $\mathcal{E} = \{(x_k, y_k, t_k, p_k)\}_{k=0}^{N_e-1}$ be the input events, where (x_k, y_k) , t_k , and $p_k \in \{-1, +1\}$ (de Blegiers et al., 2023) are the spatial coordinate, timestamp, and polarity, respectively. For view $v \in \{th, tw, hw\}$, let z^v denote the orthogonal axis ($z^{th} = x$, $z^{tw} = y$, $z^{hw} = t$). Following (Zubić et al., 2023), we can decompose the encoding function into three stages:

$$F_v(\mathcal{E}) = [F_0, \dots, F_{N_c-1}], \quad F_c = a_c(m_c(w_c(\mathcal{E}))), \quad (1)$$

where $w_c \in \mathcal{W} = \{[t_{0,k}, t_{1,k}]\}_{k=0}^{N_b-1}$ is the window function, $m_c \in \mathcal{M} = \{z_+^v, z_-^v, z^v, p, c_+, c_-, c\}$ for measurement function, and $a_c \in \mathcal{A} = \{\max, \min, \sum, \text{mean}, \text{variance}\}$ the aggregation function. Hence, assuming no out-of-bounds conditions (Fig. 3), the translation-invariance means

for any shift Δz^v :

$$F_v(\mathcal{E}|z^v) = F_v(\mathcal{E}|z^v + \Delta z^v). \quad (2)$$

This leads to find a set of conversion functions parametrized by $P = \{(w_c, a_c, m_c)\}_{c=0}^{N_c-1}$ that fulfill Eq. 2. We validate our analysis in Fig. 6, where translation-invariant w_c , a_c and m_c on temporal view map (e.g., T - H) are indeed all contributed to achieve more discriminative feature space.

Implementation. Through rigorous mathematical derivations (see Supplementary), we can identify a set of feasible, translation-invariant conversion functions:

$$\begin{aligned} P_{IV} = \{ & (w_0, \text{sum}, p), (w_0, \text{sum}, c), (w_0, \text{sum}, c_+), \\ & (w_0, \text{sum}, c_-), (w_0, \text{variance}, z^v), \\ & (w_0, \text{variance}, z_+^v), (w_0, \text{variance}, z_-^v) \}, \quad (3) \end{aligned}$$

where w_0 is a global, bin-less window. Through Eq. 3, the key findings include: (i) global window w_0 is a must; (ii) measurements $\{z^v, z_+^v, z_-^v\}$ involving z dimension satisfy Eq. 2 only when with *variance* aggregation. However, since *variance* is computationally expensive (2-order moments), we adopt 1-order $m_c = \text{sum}$ for efficiency (Tab. 4). Moreover, since c, p measurements have been proven more expressive than c_+, c_- (Fan et al., 2025), we end up selecting the compact $P_{IV}^* = \{(w_0, \text{sum}, p), (w_0, \text{sum}, c)\}$, yielding:

$$F_v = [\text{sum}(c(w_0(\mathcal{E}))), \text{sum}(p(w_0(\mathcal{E})))] \in \mathbb{R}^{2 \times U \times V}, \quad (4)$$

where $U \times V$ is the 2D resolution of view v . This obtains translation-invariant feature while maintaining efficiency.

3.3. Dual-branch and Dynamic DDCF

View Selection. Under the scheme of our global TISM representation, Zhu et al. (2019) has shown that F_{hw} doesn't record EAR-critical temporal cues. This can also be witnessed in Fig. 2 intuitively, where F_{hw} only posses spatial context of "where the actions arise" (may be useful for object detection) and spatial appearance of "what is moving" (may be useful in tasks involving multi-kind subjects beyond humans, yet without witnessed works and out-of-focus). Hence we select F_{th}, F_{tw} for efficiency. Ablations also show that including F_{hw} increases compute/parameters with negligible accuracy improvement (Tab. 6):

Formulation. Let $L = \mathcal{R}(F)$ denote a ResNet $\mathcal{R}(\cdot)$ predicting logits $L \in \mathbb{R}^C$ on F_v , C is number of classes. MVF-Net (Deng et al., 2021) applies early-concatenation with shared-branch extraction $L = \mathcal{R}([F_{th}, F_{tw}])$, which ignores dimension misalignment and informational heterogeneity (Fig. 2), motivating dual-branch extraction with late fusion:

$$L = \mathcal{F}([L_{th}, L_{tw}]), \quad L_v = \mathcal{R}_v(F_v), \quad (5)$$

where the fusion strategy $\mathcal{F}(\cdot)$ aims to exploit cross-view complementarity. The feasible $\mathcal{F}(\cdot)$ including logits averaging (LA), view-wise weighting (VW), and class-wise weighting (CW), with their formulations and attributes are detailed in Supplementary. However, even the same-class actions may exhibit distinct discriminability on different views, depending on its motion change and amplitude on horizontal (W) and vertical (H) dimension (e.g., a "Jump up" action in Fig. 7). This leads us to design a sample-wise weighting $\mathcal{F}(\cdot)$ that dynamically adapt to each sample:

$$L = w_{th}(\mathcal{E})L_{th} + w_{tw}(\mathcal{E})L_{tw}. \quad (6)$$

Implementation In principal, $w_v(\mathcal{E})$ can be learned from any feature between F_v to L . However, learning from input or middle-layer features still requires to resolve dimension misalignment not to mention the large computation, while learning from L may be insufficient in semantics for its high compactness. We therefore choose to learn dynamic weights from more informative, globally pooled $S_v \in \mathbb{R}^{512}$ before each branch's classification head that does not involve view's dimension to obtain w_{th}, w_{tw} (Fig. 3):

$$[w_{th}, w_{tw}] = \mathcal{L}(\mathcal{T}(S)) \in \mathbb{R}^{2C}. \quad (7)$$

Here, a multi-head attention block (Vaswani et al., 2017) $\mathcal{T}(\cdot)$ is applied on semantic sequence $S = [S_{th}, S_{tw}]$ to leverage its global modeling capability to model the cross-view complementarity. $\mathcal{L}(\cdot)$ is a linear layer. This is referred to "dynamic" for its consideration of sample-specific fusion weights.

3.4. Diverse Speed Variations of DTW

Formulation Real-world human actions exhibit diverse speed variations (Feichtenhofer et al., 2019), which are often neglected in existing event-based augmentations (Gu et al., 2021; Li et al., 2022; Shen et al., 2023). For an action with $T = t_e - t_0$ duration, speed variation alters temporal event density (Wu et al., 2024). Let $\mathcal{W} : \{t_k\}_{k=0}^{N_e-1} \rightarrow \{t'_k\}_{k=0}^{N_e-1}$ denote a temporal warping function mapping timestamps to warped ones, the instantaneous speed scaling factor at time t is $s(t) = \frac{d\mathcal{W}(t)}{dt}$. When $s(t) > 1$, the action decelerates locally (events become sparser); when $s(t) < 1$, it accelerates (events becomes denser). Therefore, the key to mimic diverse speed variations lies in diverse, non-uniform $\mathcal{W}(\cdot)$.

Implementation We show procedure of DTW in Algo. 1. To achieve diverse $\mathcal{W}(\cdot)$, we parameterize it through multiple non-uniform functions, including *identity*, *linear*, *power*, *exponential*, *cosine*. Each function introduces different speed profiles while maintaining temporal ordering (formulations and monotonicity guarantee are detailed in Supplementary), unlike disruptive augmentations such as FlipT⁴ (Gu et al., 2024) that invert temporal causality (e.g.,

⁴Flip events along time dimension as defined in (Gu et al.,

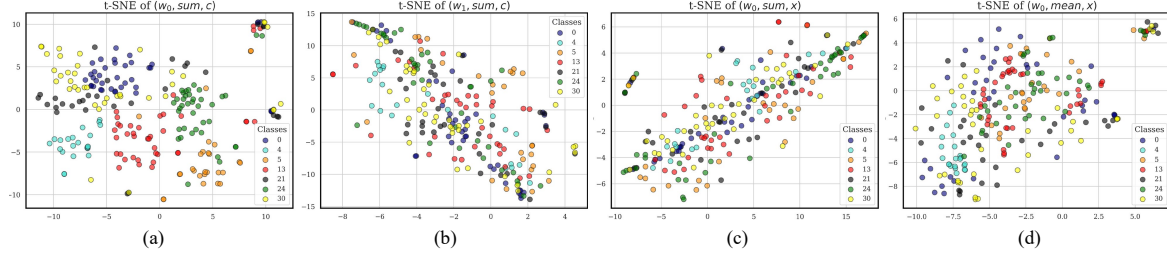


Figure 6. t-SNE visualization of $T\text{-}H$ feature maps from different encoding functions, w_1 : 2-bin. (a) vs (b) shows global encoding is better than binning. (a) vs (c),(d) shows that translation-invariant measurements and aggregations is necessary for discriminative feature space.

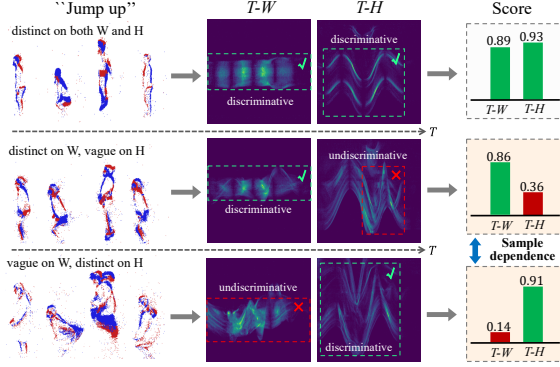


Figure 7. Predictions of two trained ResNets on different samples under a same action class. Optimal fusion may vary with samples.

Algorithm 1 Procedures of DTW augmentation.

Input: Timestamps of event sequence $\varepsilon = \{t_k\}_{k=0}^{N-1}$.
Output: Warped timestamps $\varepsilon^* = \{t_k^*\}_{k=0}^{N-1}$.

- 1: Initialize ε^* , namely $\varepsilon^* \leftarrow \varepsilon$;
- 2: Randomly select l non-overlapping intervals $\{I_j \subseteq [t_0, t_{N-1}]\}_{j=0}^l$;
- 3: **for** each interval I_j **do**
- 4: Select $\mathcal{W} \leftarrow \text{Random.choice}(identity, linear, power, exponential, cosine)$;
- 5: Sample magnitude $\{\alpha, \beta, \gamma, \eta\} \sim \mathcal{U}(a, b)$;
- 6: **for** each timestamp $t_k \in \varepsilon^*$ **do**
- 7: **if** t_k in I_j **then**
- 8: $t_k^* = \mathcal{W}(t_k, magnitude)$;
- 9: Replace t_k by t_k^* ;
- 10: **end if**
- 11: **end for**
- 12: **end for**
- 13: Adjust ε^* to connect the warped timestamps with original, non-warped timestamps to ensure continuity.

transforming “Sit down” into “Stand up”). In Fig. 8 a typical sample shows that our DTW yields local density modulation to match the intended speed variability. This observation effect aligns with the test accuracy gains in Sec. 4.3.

2024).

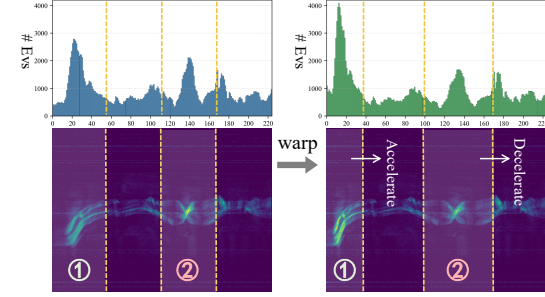


Figure 8. An example of DTW-warped $T\text{-}H$ map and the resulting event density change on 1-D event count along T dimension.

4. Experiments

4.1. Experimental Setup

Datasets. We evaluate on three recent challenging EAR datasets. *THU-EACT-50-CHL* (Gao et al., 2023) provides 2,330 samples across 50 action types captured under various lighting conditions at 346×260 resolution. *HARDVS* (Wang et al., 2024b) includes 107,646 event sequences spanning 300 action types from 5 human subjects, recorded with DAVIS346 camera at 346×260 resolution. *DailyDVS-200* (Wang et al., 2024a) consists of 22,046 sequences covering 200 daily action types from 47 human subjects, incorporating 14 distinct challenging attributes including camera motion, lighting variations, and etc..

Evaluation Metrics. With mean \pm standard deviation over five random seeds, we report Top-1 and Top-5 accuracy and measure model parameters (Params), multiply-accumulate operations (MACs), the number of floating-point operations (FLOPs) for comparison following established protocols (Gao et al., 2023; Wang et al., 2024b). The inference time $T(\text{all}) = T(\text{cpu}) + T(\text{gpu})$ is measured with batch size 1, where $T(\text{cpu})$ is the sparse-to-dense events conversion time on an AMD EPYC 7542 CPU and $T(\text{gpu})$ the network feedforward time on a RTX 3090 GPU. For translation-robustness evaluation, we inject test-time z -axis translations to events and clip into H/W range.

Table 1. Comparisons on HARDVS and DailyDVS-200. * denotes w/o augmentation and ‘-’ indicates unavailable results in existing publications, otherwise borrowed or replicating with their original configurations. MACs and T(all) are measured on HARDVS.

Method	Input Type	Backbone	Acc. on HARDVS↑		Acc. on DailyDVS-200↑		MACs↓	Params↓
			Top-1(%)	Top-5(%)	Top-1(%)	Top-5(%)		
SDT (Yao et al., 2023)	Spike	Transformer	-	-	35.43(-)	58.81(-)	-	29.3M
Spikeformer (Zhou et al., 2022)	Spike	Transformer	-	-	36.94(-)	62.37(-)	-	29.7M
C3D (Tran et al., 2015)		3D CNN	50.52(-)	56.14(-)	21.99(-)	45.81(-)	0.2G	147.2M
R2Plus1D (Tran et al., 2018)		ResNet34	49.06(-)	56.43(-)	36.06(-)	63.67(-)	40.7G	63.5M
SlowFast (Feichtenhofer et al., 2019)	Frame	ResNet50	50.63(-)	57.77(-)	41.49(-)	68.19(-)	0.7G	33.6M
TSM (Lin et al., 2019)		ResNet50	52.63(-)	60.56(-)	40.87(-)	71.46(-)	0.7G	24.3M
ACTION-Net (Wang et al., 2021)		ResNet50	46.85(-)	56.19(-)	42.61(±0.16)	71.24(±0.23)	34.7G	27.9M
EST (Gehrig et al., 2019)	Learned	ResNet34	36.51(±0.43)	42.09(±0.64)	32.23(-)	59.66(-)	2.1G	21.5M
TimeSformer (Bertasius et al., 2021)		Transformer	50.77(-)	58.70(-)	44.25(-)	74.03(-)	107.3G	121.2M
Swin-T (Liu et al., 2022)	Token	Transformer	51.91(-)	59.11(-)	48.06(-)	74.47(-)	17.5G	27.8M
GET (Peng et al., 2023)		Transformer	46.46(±0.38)	52.37(±0.19)	37.28(-)	61.59(-)	0.9G	4.5M
ESTF (Wang et al., 2024b)		ResNet18	51.22(-)	57.53(-)	24.68(-)	50.18(-)	17.6G	46.1M
CoST (Li et al., 2019)		ResNet50	50.57(±0.69)	61.38(±0.47)	36.09(±0.71)	64.45(±0.26)	9.6G	25.4M
MVFNet (Wu et al., 2021)		ResNet50	52.98(±0.41)	63.26(±0.29)	48.30(±0.27)	75.91(±0.31)	16.4G	23.6M
MVF-Net (Deng et al., 2021)	Multi-view	ResNet34&18	52.61(±0.39)	61.67(±0.07)	43.98(±0.18)	70.39(±0.95)	2.8G	33.6M
SMV-EAR*(ours)		ResNet18	55.63(±0.37)	63.56(±0.23)	50.06(±0.48)	76.47(±0.30)	1.8G	23.5M
SMV-EAR(ours)		ResNet18	59.63(±0.19)	67.56(±0.25)	54.65(±0.52)	78.28(±0.27)	1.8G	23.5M

Table 2. Comparisons on THU-EACT-50-CHL (Gao et al., 2023) dataset.

Method	Input Type	Top-1(%)↑	FLOPs↓	Params↓
HMAX SNN (Xiao et al., 2019)		32.7(-)	-	-
Motion SNN (Liu et al., 2021)	Spike	47.3(-)	-	-
EventMamba (Chen et al., 2024)		59.4(-)	3.7G	0.91M
EV-ACT (Gao et al., 2023)	Frame	58.5(-)	0.95G	21.3M
EventMG (Wu et al.)	Graph	58.8(-)	0.69G	0.77M
CoST (Li et al., 2019)		51.7(±0.32)	19.2G	25.4M
MVFNet (Wu et al., 2021)		59.6(±0.61)	32.8G	23.6M
MVF-Net (Deng et al., 2021)	Multi-View	56.5(±0.25)	5.6G	33.6M
SMV-EAR*(ours)		62.9(±0.31)	3.6G	23.5M
SMV-EAR(ours)		66.7(±0.29)	3.6G	23.5M

Implementation Details. All experiments are trained for 80 epochs in PyTorch (Paszke et al., 2019). We use AdamW optimizer (Loshchilov & Hutter, 2017) with learning rate 1e-4 and weight decay 1e-5. Following (Deng et al., 2021), T -axis are discretized into $T = 224$ and F_{th}, F_{tw} are resized into 224×224 . l of DTW is set to 4 experimentally (Supplementary). Some results replicated from other methods are obtained following their original configurations through aligned training setup with our SMV-EAR* (without augmentation), details in the Supplementary.

4.2. Comparison with the State-of-the-Arts

We compare with across different benchmarks (Gao et al., 2023; Wang et al., 2024b;a) and paradigms. As shown in Tab. 1, Tab. 2, the Spike-input frameworks (SDT, Spikeformer, HMAX SNN, Motion SNN) maintain sparsity but exhibit lower accuracy than others. The token-input frameworks (TimeSformer, V-SwinTrans) achieve higher accuracy due to Transformer’s powerful modeling capabilities but often require significant parameter and computational

Table 3. Effectiveness of three contributions in our SMV-EAR.

Components	Top-1(%)↑	FLOPs↓	Params↓	T(all)↓
MVF-Net(baseline)	56.5(±0.25)	5.6G	33.6M	14.0ms
+ TISM(w/ MVF-Net)	59.4(±0.17)	5.5G	33.6M	13.8ms
+ TISM,DDCF	62.9(±0.31)	3.6G	23.5M	10.6ms
+ All	66.7(±0.29)	3.6G	23.5M	10.6ms

cost. Our SMV-EAR consistently achieves SOTA accuracy across all datasets with +7.0% on HARDVS, +10.7% on DailyDVS-200, +10.2% on THU-EACT-50-CHL compared to the baseline method MVF-Net, while strictly controlling parameters (23.5M) and computational overhead (1.8G MACs). This validates our argument that principled SMVRL representation (TISM), architecture (DDCF) and augmentation (DTW) are more effective than merely increasing model complexity or adapting existing video or event SMVRL methods (Sec. 1).

4.3. Ablation Studies

Contributions. We conduct comprehensive ablations to validate our design choices. Tab. 3 analyzes the complementarity of our contributions on THU-EACT-50-CHL (the same applies below). With MVF-Net (Deng et al., 2021) as baseline, TISM mechanism provides significant gain (+2.9%), showing that translation-invariant representation is crucial. DDCF contributes +3.5% by enabling principled dual-branch extraction and dynamic cross-view interaction, while DTW adds +3.8% through realistic action variations. This showcases the complementarity of our three contributions.

TISM Tab. 4 validates the effectiveness of TISM (Sec. 3.2). The translation-invariant window, measurement and aggregation functions surpass those translation-variant. Moreover,

Table 4. Effectiveness of TISM. TI: translation-invariance.

w_c	m_c	a_c	TI	#C	Top-1(%)	T(cpu)
w_0	c	sum	✓	1	63.7(± 0.12)	1.2ms
w_1, w_2	c	sum	✗	2	57.6(± 0.80)	2.3ms
w_0	p	sum	✓	1	62.2(± 0.70)	1.3ms
w_3, w_4, w_5	p	sum	✗	3	55.7(± 0.14)	2.9ms
w_0	z	sum	✗	1	46.1(± 0.95)	1.6ms
w_0	z	max	✗	1	47.6(± 0.58)	1.8ms
w_0	z	mean	✗	1	49.3(± 0.80)	1.7ms
w_0	z	var.	✓	1	56.2(± 0.89)	4.1ms
w_0	c_+, c_-	sum	✓	2	62.7(± 0.45)	2.3ms
w_0	z_+, z_-	max	✗	2	45.0(± 0.81)	3.5ms
w_0	z	max,min	✗	2	46.8(± 0.18)	3.9ms
w_0	c, p, z	sum,var.	✓	3	67.1(± 0.69)	6.8ms
w_0	c, p	sum	✓	2	66.7(± 0.29)	2.5ms

while introducing $(w_0, z, \text{variance})$ channel leads to +0.4% accuracy, its events conversion is time-consuming so that fall short in efficiency. We therefore convert events with measurements c, p and aggregation *sum* for each view. We also evaluate under controlled spatial shifts in Tab. 5. where our TISM remains stable (slight degradation results from out-of-bound valid events) while MVF-Net shows clear performance drops as the shift magnitude increases. These results thoroughly validate our analysis in Sec. 3.2.

DDCF. Tab. 6 confirms the effectiveness of the proposed DDCF (Sec. 3.3). Adding F_{hw} yields limited gains and additional branch cost than the F_{th}, F_{tw} setup, this confirms our insight that omit F_{hw} map for efficient EAR. Our sample-wise weighting (SW) shows superiority over MVF-Net’s early-concatenation (EC) (Deng et al., 2021) (+10.8%), logit-averaging (LA) (+2.4%), view-wise weighting (VW) (+1.9%) and class-wise weighting (CW) (+1.5%) fusion without significantly compromising efficiency. In Tab. 7, learning w_{th}, w_{tw} from S exhibits optimal accuracy-efficiency trade-off, validating extraction timing discussed in Sec. 3.3. Implementation choices of $\mathcal{T}(\cdot)$ are ablated in Supplementary, showing 2×512 input multi-head attention achieves better modeling for cross-view complementarity.

DTW. Tab. 8 validates the effectiveness of DTW. Combination of warping functions improve the accuracy from 62.9% up to 66.7%. Other augmentation methods (Gu et al., 2021; Shen et al., 2023; Bendig et al., 2024; Dong et al., 2025) are also replicated and compared, the results reveal clear advantages (+3.3% on EventZoom (Dong et al., 2025)), validating the specificity of DTW to EAR. Notably, it can be used in conjunction with other augmentations for improvement. Beyond accuracy, Fig. 8 quantifies DTW’s intended effect on temporal density, corroborating its speed-variation modeling. **Others.** To examine the sensitivity and robustness, additional ablations are provided in Supplementary including: (i) *Architecture choice of $\mathcal{T}(\cdot)$* : comparing different implementations of $\mathcal{T}(\cdot)$, confirming a multi-head attention layer as optimal choice; (ii) *Backbone general-*

Table 5. Translation-robustness under controlled shifts on z -axis.

Method	0px	$\pm 10px$	$\pm 20px$	$\pm 30px$	$\pm 40px$
MVF-Net	56.5	51.5	51.3	49.7	46.1
SMV-EAR	66.7	66.0	65.7	65.5	64.9

Table 6. Effectiveness of dual-brach and SW fusion in DDCF.

View map	Branch	Fusion	Top-1(%)	FLOPs	Params	T(all)
F_{hw}	Single	✗	35.6(± 0.28)	1.78G	11.2M	6.1ms
F_{tw}	Single	✗	51.3(± 0.09)	1.78G	11.2M	6.1ms
F_{th}	Single	✗	60.9(± 0.37)	1.78G	11.2M	6.1ms
F_{hw}, F_{tw}	Dual	SW	48.3(± 0.81)	3.57G	23.5M	10.6ms
F_{hw}, F_{th}	Dual	SW	61.5(± 0.06)	3.57G	23.5M	10.6ms
F_{th}, F_{tw}	Dual	SW	66.7(± 0.29)	3.57G	23.5M	10.6ms
All	Triple	SW	67.0(± 0.34)	5.35G	34.7M	15.4ms
F_{th}, F_{tw}	Single	EC	55.9(± 0.56)	1.86G	11.2M	6.6ms
F_{th}, F_{tw}	Dual	LA	64.3(± 0.24)	3.57G	22.4M	10.2ms
F_{th}, F_{tw}	Dual	VW	64.8(± 0.07)	3.57G	22.4M	10.2ms
F_{th}, F_{tw}	Dual	CW	65.2(± 0.17)	3.57G	22.4M	10.2ms
F_{th}, F_{tw}	Dual	SW	66.7(± 0.29)	3.57G	23.5M	10.6ms

ization: evaluating different ResNet variants (ResNet-18, 34, 50) to verify SMV-EAR’s compact design philosophy; (iii) *Temporal resolution*: assessing performance under varying $T \in \{56, 112, 224, 448\}$ to demonstrate scalability; (iv) *Training efficiency*: comparing convergence curves and training time against baselines; (v) *Computational breakdown*: analyzing each module’s contribution to overall computation.

4.4. Visualization and Analysis.

Fine-grained Analysis. Following prior work (Wang et al., 2024a), we conduct fine-grained analysis across different action attributes in Fig. 9. While SMV-EAR* achieves superior performance on most attributes, particularly for two-person interactions (+3.3%) and sitting postures (+5.2%), it also exposes specific limitations. Camera motion remains challenging (-2.9% vs. SlowFast), as dense background events can occlude action-relevant patterns on temporal maps, degrading discriminability (Fig. 10). Interestingly, we observe that camera-induced motion exhibits near-linear streaks on temporal maps due to its globally uniform nature within short durations. This suggests a potential prior for decoupling foreground actions from background ego-motion through motion compensation or architectural inductive biases. Additionally, all methods exhibit degradation on micro actions (full-body vs. finger movements). This stems from limited spatiotemporal resolution, rendering micro-action regions informationally insufficient (Fig. 10). Potential remedies include higher-resolution sensors or adaptive attention mechanisms that selectively preserve fine-grained details. These analyses reveal principled directions for enhancing EAR under challenging real-world conditions.

Feature Visualization. To provide intuitive understanding of SMV-EAR’s learned representations, Fig. 10 visualizes

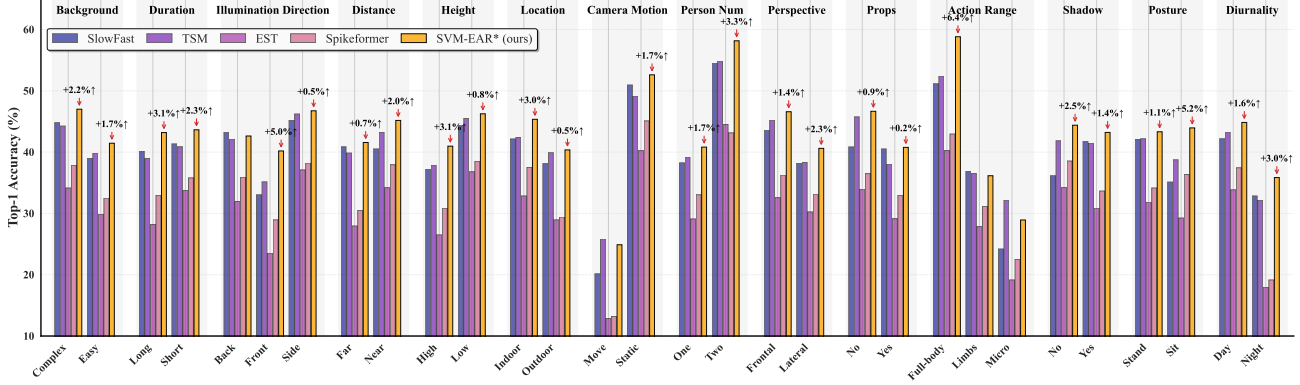


Figure 9. Comprehensive fine-grained evaluation and comparison across 14 different attribute categories on DailyDVS-200 (Wang et al., 2024a).

Table 7. Extraction timing of w_{th}, w_{tw} (with additional Res-blocks on concatenated temporal features then processed same as DDCF), $F^{(k)}$ denotes the feature after k -th Residual layer (He et al., 2016).

Temporal Feature	Top-1(%)	FLOPs	Params	T(all)
$[F_{th}, F_{tw}]$	62.5(± 0.72)	5.30G	34.6M	15.8ms
$[F_{th}^{(1)}, F_{tw}^{(1)}]$	64.5(± 0.05)	4.83G	34.5M	15.1ms
$[F_{th}^{(2)}, F_{tw}^{(2)}]$	64.6(± 0.68)	4.42G	34.0M	13.9ms
$[F_{th}^{(3)}, F_{tw}^{(3)}]$	65.8(± 0.56)	4.01G	32.0M	12.4ms
$[S_{th}, S_{tw}]$	66.7(± 0.29)	3.57G	23.5M	10.6ms
$[L_{th}, L_{tw}]$	64.4(± 0.34)	3.57G	23.6M	10.3ms

Table 8. Effectiveness of DTW, $l = 4$ intervals are applied, ‘-3D’ denotes adapting original method to raw H - W - T sparse events.

Method	Warping	Top-1(%)
w/o Aug.	<i>Id.</i>	62.9(± 0.53)
DTW	<i>+Lin.</i>	64.2(± 0.76)
DTW	<i>+Lin., Pow.</i>	65.3(± 0.23)
DTW	<i>+Lin., Pow., Exp.</i>	66.3(± 0.81)
DTW	<i>+Lin., Pow., Exp., Cos.</i>	66.7(± 0.29)
EventDrop (Gu et al., 2021)	\times	62.7(± 0.40)
EventMix-3D (Shen et al., 2023)	\times	63.1(± 0.96)
ShapeAug (Bendig et al., 2024)	\times	62.3(± 0.85)
EventZoom-3D (Dong et al., 2025)	\times	63.4(± 0.51)
DTW	<i>+Lin., Pow., Exp., Cos.</i>	66.7(± 0.29)
DTW+EventDrop	<i>+Lin., Pow., Exp., Cos.</i>	67.6(± 0.17)
DTW+EventMix-3D	<i>+Lin., Pow., Exp., Cos.</i>	67.4(± 0.09)
DTW+ShapeAug	<i>+Lin., Pow., Exp., Cos.</i>	67.2(± 0.24)
DTW+EventZoom-3D	<i>+Lin., Pow., Exp., Cos.</i>	68.1(± 0.74)

attention heatmaps overlaid on T - H and T - W maps. In successful cases, the model accurately localizes action-relevant regions, with complementary semantic cues emerging across temporal views, validating our dual-branch design. Conversely, failure cases exhibit attention diffusion under background clutter induced by camera motion or insufficient feature discriminability under micro action. These visualizations corroborate the quantitative findings in Fig. 9, offering interpretable insights into model behavior.

Feature Discriminability. Fig. 11 illustrates feature dis-

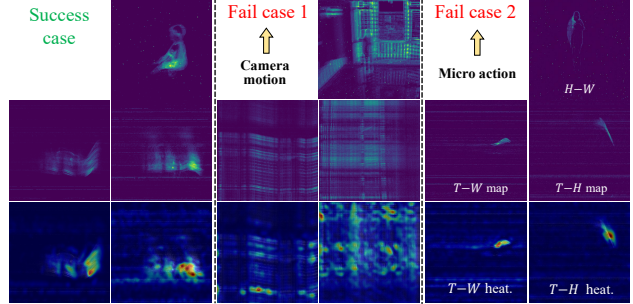


Figure 10. Heatmap visualizations. Successful cases highlight relevant regions, while failure cases show misdirected attention (in camera motion) or insufficient information (in micro action).

tributions using t-SNE and presenting confusion matrices to compare our SMV-EAR with MVF-Net (Deng et al., 2021). The t-SNE plot on action logits spanning 10 categories reveals that our method produces more distinct and well-separated clusters compared to MVF-Net, indicating superior feature discrimination. The confusion matrix on all classes further highlights the improvement of DDCF by exhibiting reduced confusion between different action categories.

5. Limitation and Future Work

Despite superior performance, there are some limitations of our method deserve clarification to benefit the future EAR research. For representation, a background noise filter could be investigated to remove the linear, action-irrelevant background streaks on T - H and T - W maps (Fig. 10), thereby promising for improved discriminability of action representation. For architecture, an insightful observation that the motion trajectories on T - H and T - W maps exhibit non-stationary dynamics characterized by time-varying frequency components, hence a frequency domain processing

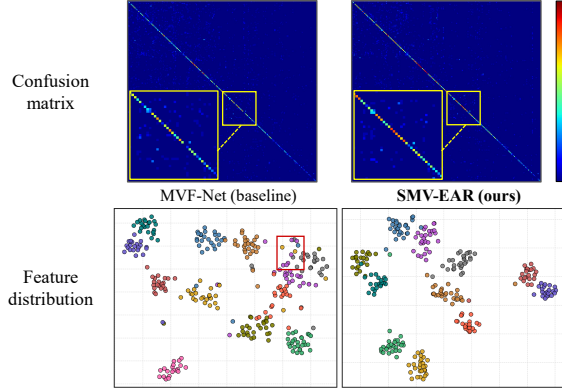


Figure 11. Visualization of confusion matrices (top) and feature distribution (bottom) of MVF-Net (Deng et al., 2021) and SMV-EAR. Ours shows improved cluster separation and reduced intra-class variance.

architecture may be useful for more effective modeling of temporal motion dynamics. For augmentation, we notice that recent EventAugment (Gu et al., 2024) has explored learning-based strategies in H - W view’s event representation, the similar paradigm could be investigated for our TISM representation to unlock further generalization ability gains. We leave a full design and evaluation to the future work.

6. Conclusion

This paper, we pioneer the first spatiotemporal multi-view representation learning (SMVRL) framework for EAR task. By revisiting key design stages spanning *representation*, *architecture* and *augmentation*, we contribute a translation-invariant spatiotemporal multi-view event representation, a dual-branch cross-view dynamic interactive network and a fundamental temporal warping data augmentation, which enhance EAR performance on various challenging benchmarks effectively from different aspects, while with strictly controlled parameters and computational overhead. This establishes our principled SMV-EAR as a novel, powerful and efficient framework paradigm for EAR task with dense event representation. Beyond the scope of this article, we hope our SMVRL EAR approach will advance the understanding of event data’s spatiotemporal dynamics, and ultimately benefit a wider spectrum of EAR-similar challenges in event-based vision in the future.

References

Bendig, K., Schuster, R., and Stricker, D. Shapeaug: Occlusion augmentation for event camera data. *arXiv preprint arXiv:2401.02274*, 2024.

Berahmand, K., Daneshfar, F., Rahmaninia, M., Haghigiat,

M., and Jalili, M. A comprehensive survey on multi-view classification: Methods, applications, and challenges. *ACM Transactions on Intelligent Systems and Technology*, 2025.

Bertasius, G., Wang, H., and Torresani, L. Is space-time attention all you need for video understanding? In *Icm*, volume 2, pp. 4, 2021.

Chakravarthi, B., Verma, A. A., Daniilidis, K., Fermuller, C., and Yang, Y. Recent event camera innovations: A survey. In *European Conference on Computer Vision*, pp. 342–376. Springer, 2024.

Chen, H. H., Huang, H., Wu, X., Liu, Y., Bai, Y., Shu, W.-J., Yang, H., and Lim, S.-N. Temporal regularization makes your video generator stronger. *arXiv preprint arXiv:2503.15417*, 2025.

Chen, J., Yang, Y., Deng, S., Teng, D., and Pan, L. Spikemamba: When snn meets mamba in event-based human action recognition. In *Proceedings of the 6th ACM International Conference on Multimedia in Asia*, pp. 1–8, 2024.

de Blegiers, T., Dave, I. R., Yousaf, A., and Shah, M. Event-transact: A video transformer-based framework for event-camera based action recognition. In *2023 IEEE/RSJ International Conference on Intelligent Robots and Systems (IROS)*, pp. 1–7. IEEE, 2023.

Deng, Y., Chen, H., and Li, Y. Mvf-net: A multi-view fusion network for event-based object classification. *IEEE Transactions on Circuits and Systems for Video Technology*, 32 (12):8275–8284, 2021.

Deng, Y., Chen, H., and Li, Y. A dynamic gcn with cross-representation distillation for event-based learning. In *Proceedings of the AAAI Conference on Artificial Intelligence*, volume 38, pp. 1492–1500, 2024.

Dong, Y., He, X., Shen, G., Zhao, D., Li, Y., and Zeng, Y. Eventzoom: A progressive approach to event-based data augmentation for enhanced neuromorphic vision. In *Proceedings of the AAAI Conference on Artificial Intelligence*, volume 39, pp. 1291–1299, 2025.

Fan, R., Hao, W., Guan, J., Rui, L., Gu, L., Wu, T., Zeng, F., and Zhu, Z. Eventpillars: Pillar-based efficient representations for event data. In *Proceedings of the AAAI Conference on Artificial Intelligence*, volume 39, pp. 2861–2869, 2025.

Feichtenhofer, C., Fan, H., Malik, J., and He, K. Slowfast networks for video recognition. In *Proceedings of the IEEE/CVF international conference on computer vision*, pp. 6202–6211, 2019.

Fey, M., Lenssen, J. E., Weichert, F., and Müller, H. Splinecnn: Fast geometric deep learning with continuous b-spline kernels. In *Proceedings of the IEEE conference on computer vision and pattern recognition*, pp. 869–877, 2018.

Gallego, G., Delbrück, T., Orchard, G., Bartolozzi, C., Taba, B., Censi, A., Leutenegger, S., Davison, A. J., Conradt, J., Daniilidis, K., et al. Event-based vision: A survey. *IEEE transactions on pattern analysis and machine intelligence*, 44(1):154–180, 2020.

Gao, Y., Lu, J., Li, S., Ma, N., Du, S., Li, Y., and Dai, Q. Action recognition and benchmark using event cameras. *IEEE Transactions on Pattern Analysis and Machine Intelligence*, 45(12):14081–14097, 2023.

Gao, Y., Lu, J., Li, S., Li, Y., and Du, S. Hypergraph-based multi-view action recognition using event cameras. *IEEE Transactions on Pattern Analysis and Machine Intelligence*, 46(10):6610–6622, 2024.

Gehrig, D., Loquercio, A., Derpanis, K. G., and Scaramuzza, D. End-to-end learning of representations for asynchronous event-based data. In *Proceedings of the IEEE/CVF international conference on computer vision*, pp. 5633–5643, 2019.

Gu, F., Sng, W., Hu, X., and Yu, F. Eventdrop: Data augmentation for event-based learning. *arXiv preprint arXiv:2106.05836*, 2021.

Gu, F., Dou, J., Li, M., Long, X., Guo, S., Chen, C., Liu, K., Jiao, X., and Li, R. Eventaugment: learning augmentation policies from asynchronous event-based data. *IEEE Transactions on Cognitive and Developmental Systems*, 16(4):1521–1532, 2024.

Hamann, F., Ghosh, S., Juárez Martínez, I., Hart, T., Kacelnik, A., and Gallego, G. Fourier-based action recognition for wildlife behavior quantification with event cameras. *Advanced Intelligent Systems*, 7(2):2400353, 2025.

He, K., Zhang, X., Ren, S., and Sun, J. Deep residual learning for image recognition. In *Proceedings of the IEEE conference on computer vision and pattern recognition*, pp. 770–778, 2016.

Li, C., Zhong, Q., Xie, D., and Pu, S. Collaborative spatiotemporal feature learning for video action recognition. In *Proceedings of the ieee/cvf conference on computer vision and pattern recognition*, pp. 7872–7881, 2019.

Li, Y., Kim, Y., Park, H., Geller, T., and Panda, P. Neuromorphic data augmentation for training spiking neural networks. In *European Conference on Computer Vision*, pp. 631–649. Springer, 2022.

Lin, J., Gan, C., and Han, S. Tsm: Temporal shift module for efficient video understanding. In *Proceedings of the IEEE/CVF international conference on computer vision*, pp. 7083–7093, 2019.

Lin, X., Liu, M., and Chen, H. Spike-har++: an energy-efficient and lightweight parallel spiking transformer for event-based human action recognition. *Frontiers in Computational Neuroscience*, 18:1508297, 2024.

Liu, Q., Xing, D., Tang, H., Ma, D., and Pan, G. Event-based action recognition using motion information and spiking neural networks. In *IJCAI*, pp. 1743–1749, 2021.

Liu, Z., Ning, J., Cao, Y., Wei, Y., Zhang, Z., Lin, S., and Hu, H. Video swin transformer. In *Proceedings of the IEEE/CVF conference on computer vision and pattern recognition*, pp. 3202–3211, 2022.

Loshchilov, I. and Hutter, F. Decoupled weight decay regularization. *arXiv preprint arXiv:1711.05101*, 2017.

Miao, S., Chen, G., Ning, X., Zi, Y., Ren, K., Bing, Z., and Knoll, A. Neuromorphic vision datasets for pedestrian detection, action recognition, and fall detection. *Frontiers in neurorobotics*, 13:38, 2019.

Neimark, D., Bar, O., Zohar, M., and Asselmann, D. Video transformer network. In *Proceedings of the IEEE/CVF international conference on computer vision*, pp. 3163–3172, 2021.

Paszke, A., Gross, S., Massa, F., Lerer, A., Bradbury, J., Chanan, G., Killeen, T., Lin, Z., Gimelshein, N., Antiga, L., et al. Pytorch: An imperative style, high-performance deep learning library. *Advances in neural information processing systems*, 32, 2019.

Peng, Y., Zhang, Y., Xiong, Z., Sun, X., and Wu, F. Get: Group event transformer for event-based vision. In *Proceedings of the IEEE/CVF International Conference on Computer Vision*, pp. 6038–6048, 2023.

Qi, C. R., Su, H., Mo, K., and Guibas, L. J. Pointnet: Deep learning on point sets for 3d classification and segmentation. In *Proceedings of the IEEE conference on computer vision and pattern recognition*, pp. 652–660, 2017a.

Qi, C. R., Yi, L., Su, H., and Guibas, L. J. Pointnet++: Deep hierarchical feature learning on point sets in a metric space. *Advances in neural information processing systems*, 30, 2017b.

Ramesh, S., Dall’Alba, D., Gonzalez, C., Yu, T., Mascagni, P., Mutter, D., Marescaux, J., Fiorini, P., and Padoy, N. Trandaugment: temporal random augmentation strategy for surgical activity recognition from videos. *International Journal of Computer Assisted Radiology and Surgery*, 18(9):1665–1672, 2023.

Rebecq, H., Horstschafer, T., and Scaramuzza, D. Real-time visual-inertial odometry for event cameras using keyframe-based nonlinear optimization. *British Machine Vision Conference*, 2017.

Ren, H., Zhou, Y., Huang, Y., Fu, H., Lin, X., Song, J., and Cheng, B. Spikepoint: An efficient point-based spiking neural network for event cameras action recognition. *arXiv preprint arXiv:2310.07189*, 2023.

Ruan, Z., Pu, N., Chen, J., Gao, S., Guo, Y., Kong, Q., Xie, Y., and Wei, Y. Few-shot event-based action recognition. *Neural Networks*, pp. 107750, 2025.

Schaefer, S., Gehrig, D., and Scaramuzza, D. Aegnn: Asynchronous event-based graph neural networks. In *Proceedings of the IEEE/CVF conference on computer vision and pattern recognition*, pp. 12371–12381, 2022.

Shen, G., Zhao, D., and Zeng, Y. Eventmix: An efficient data augmentation strategy for event-based learning. *Information Sciences*, 644:119170, 2023.

Steffen, L., Trapp, T., Roennau, A., and Dillmann, R. Efficient gesture recognition on spiking convolutional networks through sensor fusion of event-based and depth data. In *2024 IEEE International Conference on Robotics and Automation (ICRA)*, pp. 345–352. IEEE, 2024.

Sun, J., Zhang, Q., Wang, J., Cao, J., and Xu, R. Event masked autoencoder: Point-wise action recognition with event-based cameras. *arXiv preprint arXiv:2501.01040*, 2025.

Sun, L., Zhang, Y., Cheng, J., and Lu, H. Asynchronous event processing with local-shift graph convolutional network. In *Proceedings of the AAAI Conference on Artificial Intelligence*, volume 37, pp. 2402–2410, 2023.

Tavanaei, A., Ghodrati, M., Kheradpisheh, S. R., Masquelier, T., and Maida, A. Deep learning in spiking neural networks. *Neural networks*, 111:47–63, 2019.

Tran, D., Bourdev, L., Fergus, R., Torresani, L., and Paluri, M. Learning spatiotemporal features with 3d convolutional networks. In *Proceedings of the IEEE international conference on computer vision*, pp. 4489–4497, 2015.

Tran, D., Wang, H., Torresani, L., Ray, J., LeCun, Y., and Paluri, M. A closer look at spatiotemporal convolutions for action recognition. In *Proceedings of the IEEE conference on Computer Vision and Pattern Recognition*, pp. 6450–6459, 2018.

Vaswani, A., Shazeer, N., Parmar, N., Uszkoreit, J., Jones, L., Gomez, A. N., Kaiser, Ł., and Polosukhin, I. Attention is all you need. *Advances in neural information processing systems*, 30, 2017.

Wang, Q., Xu, Z., Lin, Y., Ye, J., Li, H., Zhu, G., Ali Shah, S. A., Bennamoun, M., and Zhang, L. Dailydvs-200: A comprehensive benchmark dataset for event-based action recognition. In *European Conference on Computer Vision*, pp. 55–72. Springer, 2024a.

Wang, X., Wu, Z., Jiang, B., Bao, Z., Zhu, L., Li, G., Wang, Y., and Tian, Y. Hardvs: Revisiting human activity recognition with dynamic vision sensors. In *Proceedings of the AAAI conference on artificial intelligence*, volume 38, pp. 5615–5623, 2024b.

Wang, X., Wang, H., Wang, S., Chen, Q., Jin, J., Song, H., Jiang, B., and Li, C. Rgb-event based pedestrian attribute recognition: A benchmark dataset and an asymmetric rwkv fusion framework. *arXiv preprint arXiv:2504.10018*, 2025.

Wang, Y., Sun, Y., Liu, Z., Sarma, S. E., Bronstein, M. M., and Solomon, J. M. Dynamic graph cnn for learning on point clouds. *ACM Transactions on Graphics (tog)*, 38(5):1–12, 2019.

Wang, Z., She, Q., and Smolic, A. Action-net: Multipath excitation for action recognition. In *Proceedings of the IEEE/CVF conference on computer vision and pattern recognition*, pp. 13214–13223, 2021.

Wu, H., Ma, X., and Li, Y. Transformer-based multiview spatiotemporal feature interactive fusion for human action recognition in depth videos. *Signal Processing: Image Communication*, 131:117244, 2025.

Wu, S., Jin, L., Feng, H., and Hu, B. Eventmg: Efficient multilevel mamba-graph learning for spatiotemporal event representation. In *The Thirty-ninth Annual Conference on Neural Information Processing Systems*.

Wu, S., Sheng, H., Feng, H., and Hu, B. Egsst: Event-based graph spatiotemporal sensitive transformer for object detection. *Advances in Neural Information Processing Systems*, 37:120526–120548, 2024.

Wu, W., He, D., Lin, T., Li, F., Gan, C., and Ding, E. Myfnet: Multi-view fusion network for efficient video recognition. In *Proceedings of the AAAI conference on artificial intelligence*, volume 35, pp. 2943–2951, 2021.

Wu, Y., Deng, L., Li, G., Zhu, J., and Shi, L. Spatiotemporal backpropagation for training high-performance spiking neural networks. *Frontiers in neuroscience*, 12:331, 2018.

Xiao, R., Tang, H., Ma, Y., Yan, R., and Orchard, G. An event-driven categorization model for aer image sensors using multispike encoding and learning. *IEEE transactions on neural networks and learning systems*, 31(9):3649–3657, 2019.

Xie, B., Deng, Y., Shao, Z., Liu, H., and Li, Y. Vmv-gcn: Volumetric multi-view based graph cnn for event stream classification. *IEEE Robotics and Automation Letters*, 7 (2):1976–1983, 2022.

Xie, B., Deng, Y., Shao, Z., Xu, Q., and Li, Y. Event voxel set transformer for spatiotemporal representation learning on event streams. *IEEE Transactions on Circuits and Systems for Video Technology*, 2024.

Yao, M., Hu, J., Zhou, Z., Yuan, L., Tian, Y., Xu, B., and Li, G. Spike-driven transformer. *Advances in neural information processing systems*, 36:64043–64058, 2023.

Zhou, J., Zheng, X., Lyu, Y., and Wang, L. Exact: Language-guided conceptual reasoning and uncertainty estimation for event-based action recognition and more. In *Proceedings of the IEEE/CVF Conference on Computer Vision and Pattern Recognition*, pp. 18633–18643, 2024.

Zhou, Z., Zhu, Y., He, C., Wang, Y., Yan, S., Tian, Y., and Yuan, L. Spikformer: When spiking neural network meets transformer. *arXiv preprint arXiv:2209.15425*, 2022.

Zhu, A. Z., Yuan, L., Chaney, K., and Daniilidis, K. Unsupervised event-based learning of optical flow, depth, and egomotion. In *Proceedings of the IEEE/CVF conference on computer vision and pattern recognition*, pp. 989–997, 2019.

Zubić, N., Gehrig, D., Gehrig, M., and Scaramuzza, D. From chaos comes order: Ordering event representations for object recognition and detection. In *Proceedings of the IEEE/CVF International Conference on Computer Vision*, pp. 12846–12856, 2023.